LPSC14305
UCD-2014-004

Light Higgs bosons in Two-Higgs-Doublet Models

Jeremy Bernon[1],* John F. Gunion[2],† Yun Jiang[2],‡ and Sabine Kraml[1]§

(1) Laboratoire de Physique Subatomique et de Cosmologie,

Université Grenoble-Alpes, CNRS/IN2P3,

53 Avenue des Martyrs, F-38026 Grenoble, France and

(2) Department of Physics, University of California, Davis, CA 95616, USA

arXiv:1412.3385v2 [hep-ph] 23 Jan 2015

We explore the possibilities in two-Higgs-doublet models (2HDMs) of Type I and Type II for Higgs states with mass below about 60 GeV, *i.e.* less than half of the $\sim$ 125 GeV mass of the observed SM-like Higgs boson. We identify the latter as either the lighter or the heavier CP-even state, h or H, and employ scans of the 2HDM parameter space taking into account all relevant theoretical and experimental constraints, including the most up-to-date Higgs signal strength measurements. We find that, in both Type I and Type II models, such light Higgs states are phenomenologically viable and can lead to interesting signatures. Part of the relevant parameter space may be testable with the existing 8 TeV LHC data, *e.g.* by looking for direct production of the light state via gg-fusion or $b\bar{b}$-associated-production using its $\tau^+\tau^-$ and $\mu^+\mu^-$ decays at low invariant mass.

PACS numbers: 12.60.Fr, 14.80.Ec, 14.80.Fd

Keywords: Higgs physics, 2-Higgs-Doublet Model, LHC

*jeremy.bernon@lpsc.in2p3.fr

†jfgunion@ucdavis.edu

‡yunjiang@ucdavis.edu

§sabine.kraml@lpsc.in2p3.fr

I. INTRODUCTION

Now that a new particle has been discovered at the LHC with properties close to those of the SM Higgs boson, it is important to assess all possibilities for other Higgs-like states that may have escaped detection at Run 1 of the LHC. Two-Higgs-doublet models (2HDMs — we consider Type I and Type II models) are an especially simple and appealing framework for such considerations. They contain five Higgs bosons (the CP-even h and H, the CP-odd A, and the charged states $H^\pm$) where the h or H can have SM-like couplings and may therefore be identified with the observed 125 GeV state — denoted $h125$ and $H125$, respectively. One often considered limit of the 2HDM is the decoupling limit [1] in which $m_A, m_H, m_{H^\pm}$ are all large, in which case the h is very SM-like.

A SM-like h or H can however also be obtained in the alignment limit without the masses of the other Higgs being large. Here, we address the seemingly extreme case in which the h (H) is the SM-like 125 GeV state and the A (A and/or h) are lighter than 125 GeV, in particular light enough that the SM-like state can decay into them. Such decays generically have a large branching ratio (early references are [2], [3] and [4]) and would conflict with Higgs precision data unless the Higgs-to-Higgs-pair branching ratio is below about 0.1–0.3 [5], depending on the model.[1]

Only by tuning the model parameters so that the SM-like Higgs has very small coupling to a pair of lighter Higgs bosons can such a small branching ratio be achieved. Nonetheless, this is a parameter space window that cannot yet be excluded and that has many interesting special features, including rather large predicted cross sections for direct production of the light Higgs boson(s) — cross sections that might even be testable using the existing LHC 8 TeV data. The goal of this paper is to delineate these scenarios and their special properties.

We note that these scenarios are not achievable in the MSSM because of the strong interrelations of the Higgs potential parameters required by supersymmetry; a light A is simply not consistent within the MSSM when the h has mass 125 GeV (unless the Higgs sector is CP-violating). MSSM scenarios in which the H has mass of 125 GeV and m_A, m_h are below m_H have been constructed [7], but those to date do not have $m_A, m_h < 125/2$ GeV. In the NMSSM, scenarios with a light a_1 and/or h_1 are possible in light of the current data

[1] A large survey of exotic Higgs decays is available in [6].

[8–11] but are not the subject of this paper — they typically imply small cross sections for production of the light Higgs boson.[2]

The key consideration for this study is the magnitude of the coupling of the SM-like Higgs to a pair of the other Higgs bosons. We employ the formulae found in [1] extensively. There one finds the following results.

$$g_{hAA} = -v\big[\lambda_T \sin(\beta-\alpha) - \lambda_U \cos(\beta-\alpha)\big]\,, \tag{1}$$

$$g_{HAA} = -v\big[\lambda_T \cos(\beta-\alpha) + \lambda_U \sin(\beta-\alpha)\big]\,, \tag{2}$$

$$\begin{aligned} g_{Hhh} = 3v\big[&\lambda \cos(\beta-\alpha)\left(-\tfrac{2}{3} + s^2_{\beta-\alpha}\right) - \widehat{\lambda}\sin(\beta-\alpha)(1-3c^2_{\beta-\alpha}) \\ &+(2\lambda_A - \lambda_T)\cos(\beta-\alpha)\left(\tfrac{1}{3} - s^2_{\beta-\alpha}\right) - \lambda_U c^2_{\beta-\alpha}\sin(\beta-\alpha)\big] \end{aligned} \tag{3}$$

where

$$\lambda_T = \tfrac{1}{4}s^2_{2\beta}(\lambda_1+\lambda_2) + \lambda_{345}(s^4_\beta + c^4_\beta) - 2\lambda_5 - s_{2\beta}c_{2\beta}(\lambda_6-\lambda_7)\,, \tag{4}$$

$$\lambda_U = \tfrac{1}{2}s_{2\beta}(s^2_\beta\lambda_1 - c^2_\beta\lambda_2 + c_{2\beta}\lambda_{345}) - \lambda_6 s_\beta s_{3\beta} - \lambda_7 c_\beta c_{3\beta}\,. \tag{5}$$

In the above, $\tan\beta = v_2/v_1$ is the ratio of the vevs of the two Higgs doublets, $v \equiv \sqrt{v_1^2+v_2^2} = 246$ GeV and α is the mixing angle required to diagonalize the CP-even mass-squared matrix (see [1] for details).

In terms of g_{YXX}, where Y is the SM-like Higgs and X is the A for $Y=h$ and either the A or h for $Y=H$, we find

$$R(XX) \equiv \frac{\Gamma(Y\to XX)}{\Gamma(Y\to bb)} = \frac{1}{12}\left(\frac{g_{YXX}v}{m_Y m_b}\right)^2 \frac{\beta(m_X)}{\beta^3(m_b)} \tag{6}$$

with $\beta(m_X) = \sqrt{1-4m_X^2/m_Y^2}$. Taking $m_Y = 125$ GeV and assuming purely SM-like couplings for Y, one finds that $R(XX) \lesssim \frac{5}{6}$ (equivalent to $\mathrm{BR}(Y\to XX) < 0.3$) requires $|g_{YXX}| \lesssim 17$ GeV for $m_X = 62$ GeV, which goes down to $|g_{YXX}| \lesssim 6$ GeV for $m_X \simeq 10-40$ GeV. We will see that such a small g_{YXX} is a very strong constraint — without parameter tuning $|g_{YXX}|$ is most naturally of the order of a TeV.

In the following, we consider $Y=h$ in Section II and $Y=H$ in Section III. We begin each of these sections by discussing the special parameter choices required in order to avoid too

[2] NMSSM scenarios with a light a_1 and/or h_1 that appears in the decay of a SM-like Higgs (*e.g.* $h_2\to a_1a_1$, where h_2 is SM-like) have a long history, the original paper being [12].

large Higgs-to-Higgs-pair branching ratio(s) for the 125 GeV state and then proceed to the associated phenomenology. Our procedure for exploring the 2HDM parameter space is the same as in [13, 14]. All points that are retained obey the constraints from stability, unitarity and perturbativity (SUP), electroweak precision tests (STU), LEP searches, as well as the limits imposed by non-observation at the LHC of any Higgs bosons other than the SM-like one at 125 GeV. Regarding constraints from the Higgs signal strength measurements at 125 GeV, for each of the observed Higgs decay modes ($\gamma\gamma$, $WW^{(*)}$, $ZZ^{(*)}$, $b\bar{b}$, $\tau\bar{\tau}$) we require agreement at the 95% CL with the ATLAS+CMS combined signal strength ellipse in the (ggF+ttH) and (VBF+VH) plane, as explained in [13]. These signal strength ellipses have been determined from a fit with `Lilith 1.0.1` [5, 15], including the lastest experimental results as of October, 2014. In the plots below we consider only scan points that pass all these constraints.[3]

II. THE $m_h \sim 125$ GeV CASE

Using Eqs. (1), (4), (5) and the relationships of the λ_i to the physical Higgs masses and the Higgs mixing parameter, m_{12}^2, in the scalar potential (see [1]), one finds the following result for the hAA coupling:

$$g_{hAA} \;=\; \frac{1}{2v}\left[\left(2m_A^2 - m_h^2\right)\frac{\cos(\alpha-3\beta)}{\sin 2\beta} + \left(8m_{12}^2 - \sin 2\beta\left(2m_A^2+3m_h^2\right)\right)\frac{\cos(\beta+\alpha)}{\sin^2 2\beta}\right] \quad (7)$$

Let us begin by taking the SM limit, $\sin(\beta-\alpha)=1$, in the formula above:

$$g_{hAA} = -\frac{2m_A^2 + m_h^2 - 2\hat{m}_{12}^2}{v} \quad (8)$$

where $\hat{m}_{12}^2 = m_{12}^2 \sec\beta \csc\beta$ and m_{12}^2 can be positive or negative. Given that $|g_{hAA}|$ must be very small to have small BR($h \to AA$), we see that in this limit $m_h^2 \sim -2m_A^2 + 2\hat{m}_{12}^2$ is required.[4] While there is no symmetry that motivates this particular choice, it can certainly be satisfied for appropriately modest $\hat{m}_{12}^2$ and we find many allowed points of this nature.

The interrelations of the parameters in this region are illustrated in Fig. 1. The figure shows the combined impact of perturbativity and the requirement of small BR($h \to AA$).

[3] In [13, 14], we also required that the "feed down" of heavier Higgs states to the signal at 125 GeV be not too large. In the scenarios investigated in this paper, such feed down processes are irrelevant.

[4] Without this cancellation, when the g_{hAA} coupling is large, one may still suppress the $h \to AA$ decay by minimizing its phase space; however, this is not the case of interest in this study.

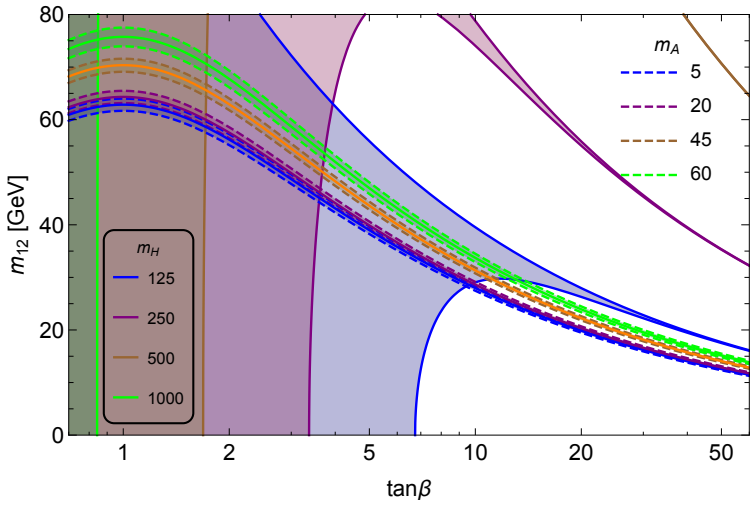

FIG. 1: For $\sin(\beta-\alpha)=1$, we show the regions of m_{12} vs. $\tan\beta$ parameter space consistent with perturbativity for various m_H values (see in-figure color code in lower-left corner). Also shown are the narrow regions for which $\mathrm{BR}(h\to AA)<0.3$, assuming h is the SM-like Higgs at 125 GeV with a total decay width of 4.07 MeV, for the indicated values of m_A shown in the upper-right corner. The figure applies to both the Type I and Type II 2HDM. The perturbatively acceptable region also extends to $m_{12}^2<0$, but this region is not plotted since Eq. (8) would give large $|g_{hAA}|$ and, therefore, large $\mathrm{BR}(h\to AA)$ if m_{12}^2 were negative.

The large solid filled regions are those allowed by perturbativity for various different values of m_H (as indicated by the color code in the lower-left corner of the plot). The regions surrounded by dashed lines are those consistent with $\mathrm{BR}(h\to AA)\leq 0.3$, with the central solid line corresponding to $\mathrm{BR}(h\to AA)=0$ (or equivalently g_{hAA}=0), for the various m_A values coded as shown in the upper-right corner of the plot. We see that the higher the value of m_H, the smaller the $\tan\beta$ that is required by perturbativity. Imposing both perturbativity and $\mathrm{BR}(h\to AA)\leq 0.3$ strongly constrains m_{12} within the allowed $\tan\beta$ range (note: $m_{12}\equiv \mathrm{sgn}(m_{12}^2)\sqrt{|m_{12}^2|}$). Roughly, $m_{12}\approx 30-100$ GeV and $\tan\beta<15$ are the interesting ranges to scan over for this solution.

Deviating from the strict SM limit, there is also another parameter region that gives small $|g_{hAA}|$ through a cancellation between the first and second terms in Eq. (7) (or, equivalently, between the m_{12}^2 and non-m_{12}^2 terms in this equation). This can be achieved when $\sin(\beta+\alpha)$ is close to one and allows also for larger m_{12}^2. As described in [16], $\sin(\beta+\alpha)\sim 1$ can be

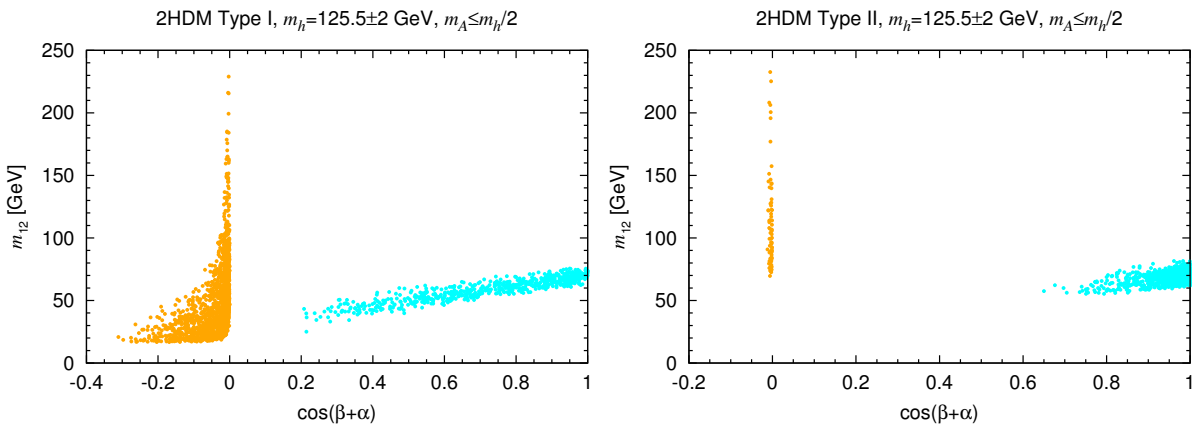

FIG. 2: Phenomenologically viable points with $m_A \leq m_h/2$ in the m_{12} vs. $\cos(\beta+\alpha)$ plane, for 2HDM Type I (left) and Type II (right). The cyan points have $\sin(\beta-\alpha) \sim 1$, $\cos(\beta-\alpha) > 0$ and modest m_{12}, as for the $\sin(\beta-\alpha) = 1$ allowed region seen in Fig. 1, while the orange points have $\sin(\beta+\alpha) \sim 1$, small $\cos(\beta+\alpha) < 0$ and $\tan\beta > 5$.

consistent with the h being SM-like so long as $\tan\beta$ is not too small. In particular, one finds in this limit

$$C_V = \sin(\beta-\alpha) \to \frac{\tan^2\beta - 1}{\tan^2\beta + 1}\,, \tag{9}$$

where C_V is the magnitude of the hVV coupling relative to the SM value. One obtains $C_V \gtrsim 0.95$ once $\tan\beta \gtrsim 6$, *i.e.* sufficiently close to unity for consistency with Higgs data from the LHC. Note, however, that one cannot actually use exactly $\sin(\beta+\alpha) = 1$. This is because if both $\sin(\beta-\alpha) \to 1$ and $\sin(\beta+\alpha) \to 1$, then $\beta \to \pi/2$ and $\alpha \to 0$, for which g_{hAA} becomes too large. Indeed, in the limit of $\sin(\beta+\alpha) = 1$, we obtain

$$g_{hAA} = \frac{2m_A^2 - m_h^2}{v}\cos 2\beta\,, \tag{10}$$

which is too large given that $\cos 2\beta \sim -1$ for $\tan\beta \gtrsim 6$.

An overall view of the allowed low-m_A points in m_{12} vs. $\cos(\beta+\alpha)$ space for the Type I and Type II 2HDMs is provided by Fig. 2, and in the $\tan\beta$ vs. $\sin\alpha$ plane in Fig. 3. The cyan points have $\sin(\beta-\alpha) \sim 1$, $\cos(\beta+\alpha) > 0$ and modest m_{12}, as for the $\sin(\beta-\alpha) = 1$ allowed region seen in Fig. 1, while the orange points are those with $\sin(\beta+\alpha) \sim 1$, small $\cos(\beta+\alpha) < 0$, $\tan\beta > 5$ and $m_{12} > 0$. (The opposite case with $m_{12} < 0$ and $\cos(\beta+\alpha) > 0$ could also lead to the necessary cancellations in Eq. (7) but turns out to be excluded by the 125 GeV Higgs signal constraints.) In Fig. 3, points to the right of the $\sin(\beta+\alpha) = 1$

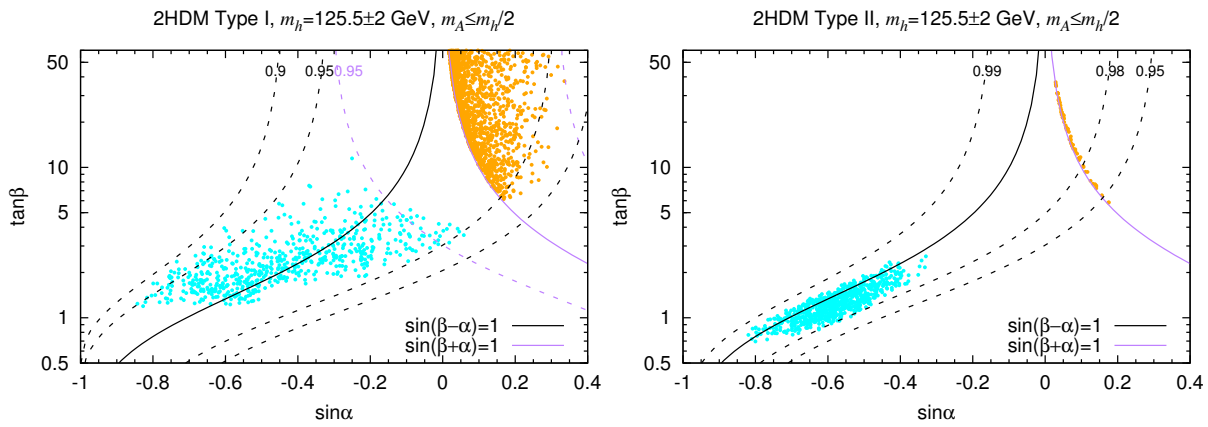

FIG. 3: Same as Fig. 2 but in the $\tan\beta$ vs. $\sin\alpha$ plane. The solid black and purple lines indicate $\sin(\beta-\alpha)=1$ and $\sin(\beta+\alpha)=1$, respectively. The dashed black (purple) lines are iso-contours of values of $\sin(\beta-\alpha)$ ($\sin(\beta+\alpha)$) as indicated on the plots.

curve have $\cos(\beta+\alpha)<0$ and those to the left have $\cos(\beta+\alpha)>0$. The requirement of small g_{hAA} (coupled with $m_{12}>0$) thus creates a very sharp boundary between acceptable vs. non-acceptable parameter points. One should also note that the $\sin(\beta+\alpha)\sim 1$ points mostly (entirely) have $\sin\alpha>0$ for Type I (Type II). Consequently, in the Type II model the orange points correspond to the "wrong-sign" Yukawa coupling $C_D^h\sim -1$ [17], whereas the cyan points have $C_D^h>0$.

For completeness we show in Fig. 4 the explicit values of $\mathrm{BR}(h\to AA)$ vs. g_{hAA} for the allowed points. We see that g_{hAA} is indeed tightly constrained to small values of the order of 5 GeV. Note that the allowed range for $\mathrm{BR}(h\to AA)$ is different for Type I and Type II models because of the different structure of the h couplings to fermions. As an aside we also note that agreement with the individual 95% CL signal strength ellipses allows for slightly higher $\mathrm{BR}(h\to AA)$ than a global fit, which would restrict $\mathrm{BR}(h\to AA)<0.16$ (0.26) in Type I (Type II) at 95% CL.

Having understood the constraints on this scenario, we now pursue the implications for LHC phenomenology. In Fig. 5 we plot the reduced couplings (relative to their SM values) of h to gluons and to photons, C_g^h vs. C_γ^h. The suppressed values of C_γ^h come from the negative contribution of the charged Higgs to the $h\gamma\gamma$ one-loop coupling. In the limit of $\sin(\beta-\alpha)=1$,

$$g_{hH^\pm H^\pm}=g_{hAA}-(\lambda_5-\lambda_4)v=g_{hAA}-2(m_{H^\pm}^2-m_A^2)/v\,. \tag{11}$$

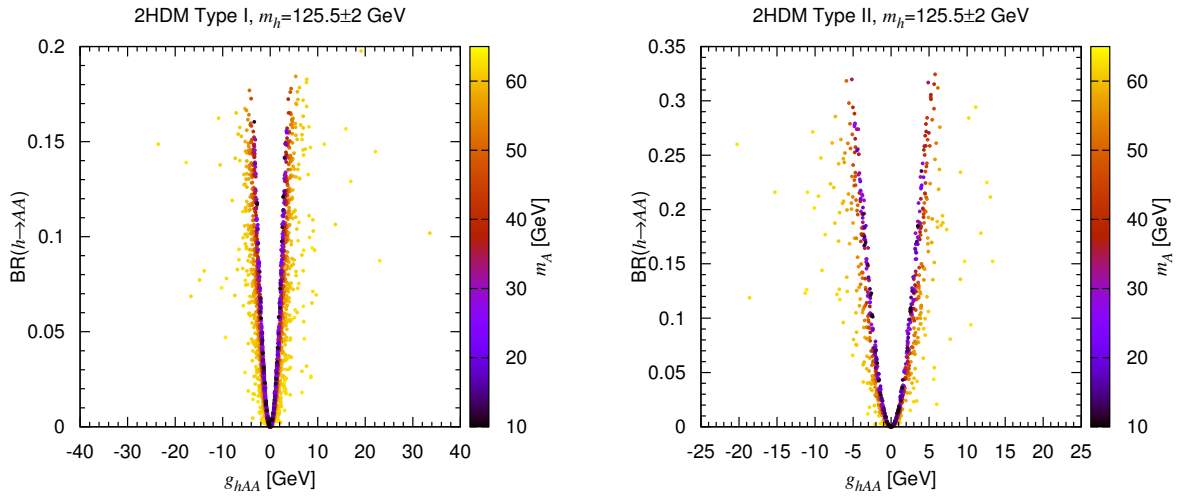

FIG. 4: Allowed points in the BR($h \to AA$) vs. g_{hAA} plane, on the left for Type I, on the right for Type II. The value of m_A is colour-coded as indicated by the scales on the right of the plots.

The first term, g_{hAA}, has to be small as discussed above and the second term is always negative because $m_{H^\pm} \gtrsim 90$ GeV (300 GeV) in Type I (Type II). The relation between C_γ^h and BR($h \to AA$) is shown in Fig. 6. While in Type I the allowed value of BR($h \to AA$) increases with C_γ^h, the trend is the opposite in Type II though with a much less pronounced correlation.

To illustrate the impact on observables, we plot in Fig. 7 the signal strengths μ (relative to the SM) for $gg \to h \to VV$ ($V = W, Z$) versus $gg \to h \to \gamma\gamma$, denoted as $\mu_{gg}^h(VV)$ vs. $\mu_{gg}^h(\gamma\gamma)$. Our first observation is that $\mu_{gg}^h(\gamma\gamma)$ is suppressed for all points in Type I as well as for the orange points in Type II. The deviations from the SM predictions of unity are of course consistent with current data, since this was a requirement of the scan, but it is obvious that future higher precision measurements will strongly constrain these scenarios. Remarkably — and in contrast to the case when $m_A > m_h/2$ — it is impossible to simultaneously achieve $\mu_{gg}^h(\gamma\gamma) = 1$ and $\mu_{gg}^h(VV) = 1$ in either Type I or Type II when $m_A \leq m_h/2$. (See Fig. 2 of [14] for comparison with the general case.) Thus, this scenario will be excluded should the Higgs observations converge sufficiently close to the SM expectations.

Figure 8 shows BR($h \to AA$) vs. signal strength $\mu_{gg}^h(\gamma\gamma)$. From the left plot we can directly see that in Type I a precise measurement of this signal strength gives an upper bound on the allowed $h \to AA$ branching ratio. If $\mu_{gg}^h(\gamma\gamma)$ is measured to be within 10% of unity, this means BR($h \to AA$) $\lesssim 0.01$. Conversely, a measurement of $\mu_{gg}^h(\gamma\gamma) \simeq 1$ combined

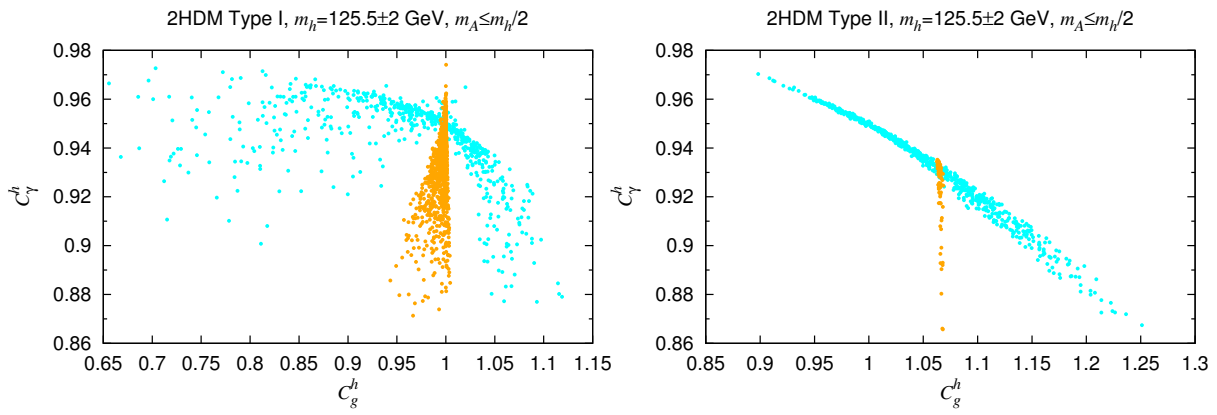

FIG. 5: As Fig. 2 but for C_γ^h vs. C_g^h.

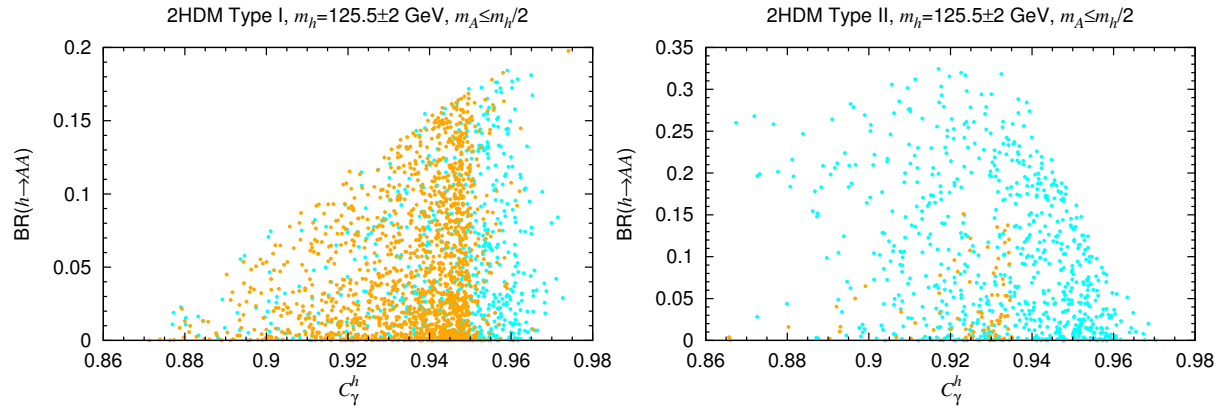

FIG. 6: As Fig. 2 but for BR($h \to AA$) vs. C_γ^h.

with detection of $h \to AA$ decays implies that the Type II model is strongly preferred and that the wrong-sign Yukawa solution is excluded.

Let us now turn to the question of the size of the cross sections for A production with decays to the potentially observable $\tau\tau$ and $\mu\mu$ final states. Figure 9 shows the gg fusion and $b\bar{b}$ associated production cross sections at $\sqrt{s} = 8$ TeV times BR($A \to \tau\tau$). As can be seen, the $A \to \tau\tau$ signal can have quite substantial cross sections over the whole mass range considered. The cross sections for the $A \to \mu\mu$ signal have exactly the same shape but are about a factor of 100 lower. For reference, naive estimates suggest that, before cuts and efficiencies, for the existing 8 TeV dataset with integrated luminosity of $L \simeq 20$ fb^{-1}, a cross section of order 10 pb (200,000 events) should be observable in the $\tau\tau$ final state while 0.1 pb (2000 events) should be observable in the $\mu\mu$ final state, especially in the case of $b\bar{b}$

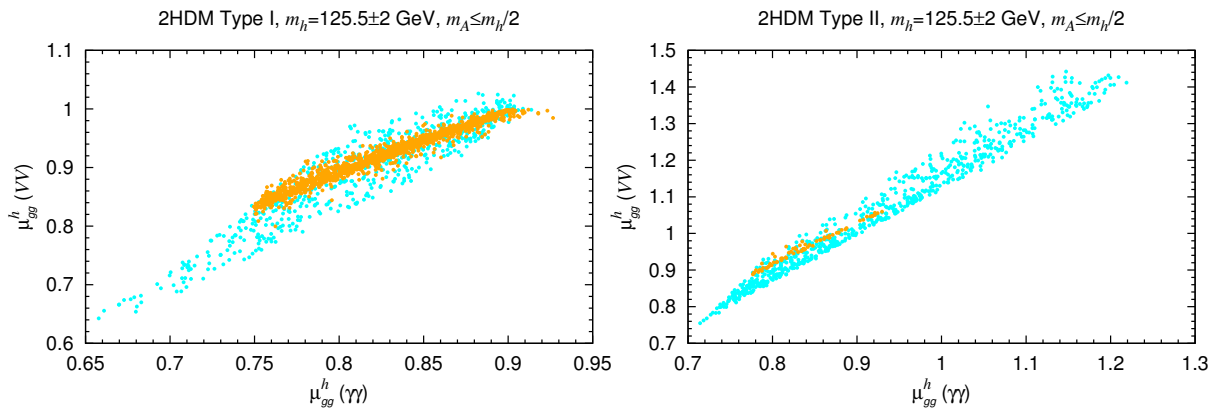

FIG. 7: Signal strengths $\mu^h_{gg}(VV)$ vs. $\mu^h_{gg}(\gamma\gamma)$ for the Type I and Type II models. The orange points are, as for previous plots, the points with $\sin(\beta+\alpha) \sim 1$.

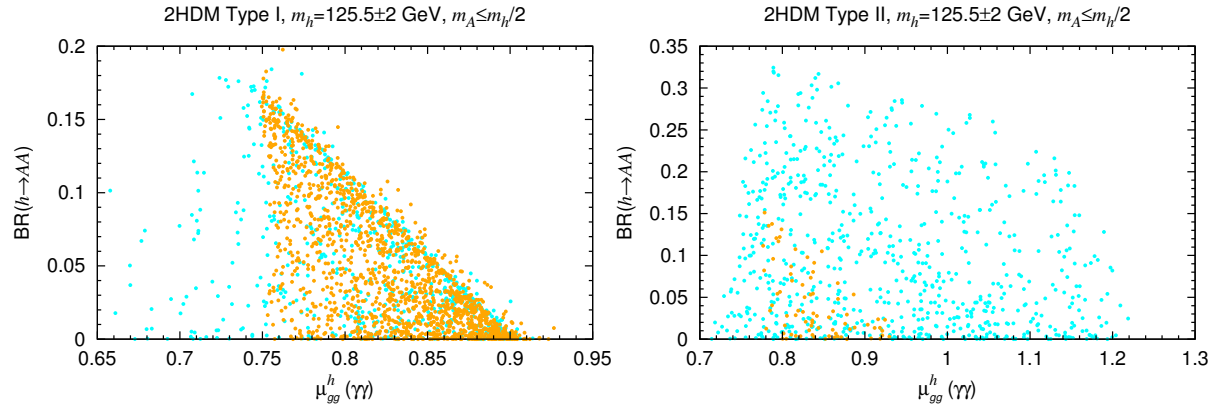

FIG. 8: BR($h \to AA$) vs. $\mu^h_{gg}(\gamma\gamma)$ for the Type I and Type II models.

associated production by using modest p_T b-tagging. From Fig. 9, we observe that these levels are reached in the case of Type II for essentially the entire $m_A \le m_h/2$ region in the case of gg fusion and for the orange points in the case of $b\bar{b}$ associated production.[5] Indeed, the cross sections for the orange points are really very large and should produce readily observable peaks. In the case of the Type I 2HDM, many of the cyan points have gg fusion cross sections at the probably observable 10 pb (0.1 pb) level in the $\tau\tau$ ($\mu\mu$) final states, but the orange points have cross sections that are almost certainly too small for detection

[5] Recall from Fig. 3 that the orange points can have high $\tan\beta$ while the cyan points have quite modest $\tan\beta$ values. This implies that the $b\bar{b}$ coupling in the Type I (Type II) model is suppressed (enhanced). As a result, the orange points have the smallest (largest) cross sections in the case of Type I (Type II).

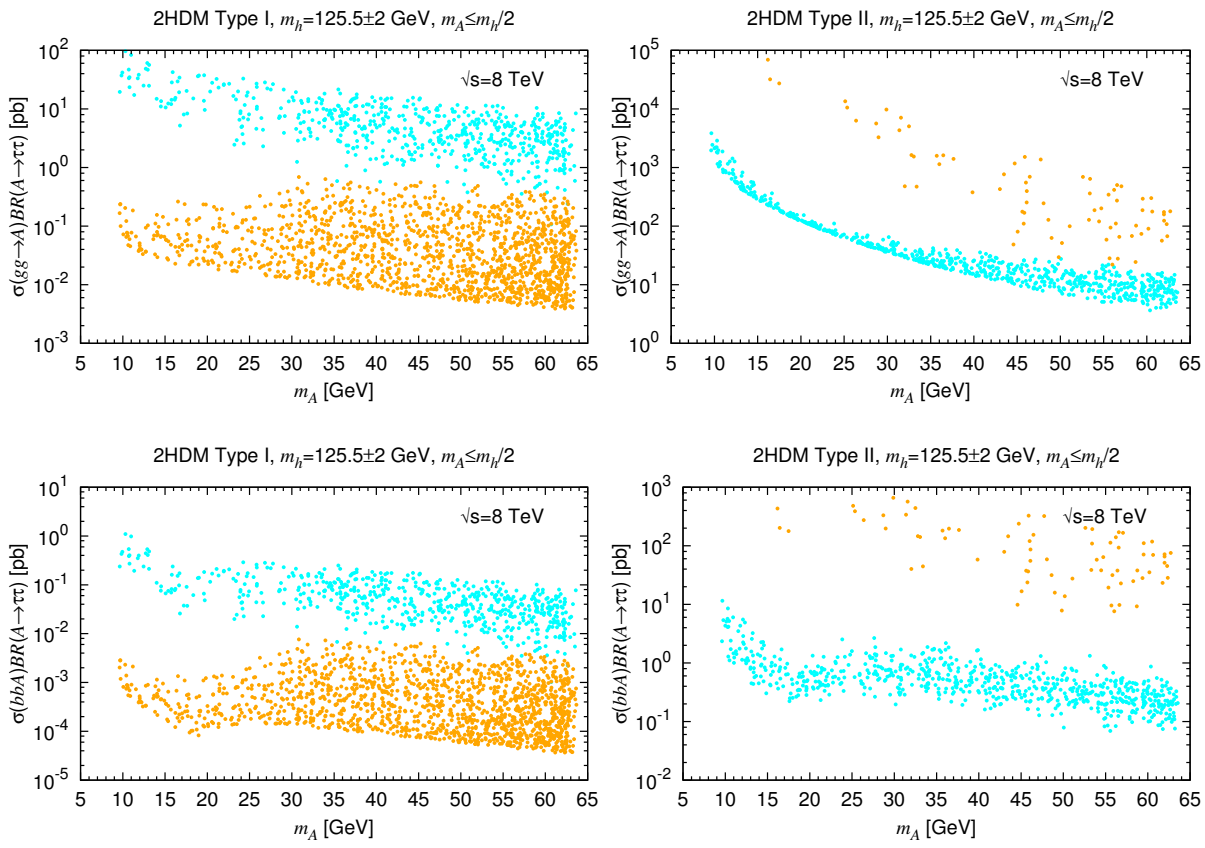
2HDM Type I, m_h=125.5±2 GeV, $m_A \leq m_h/2$
2HDM Type II, m_h=125.5±2 GeV, $m_A \leq m_h/2$
√s=8 TeV
$\sigma(gg \to A)BR(A \to \tau\tau)$ [pb]
$\sigma(bbA)BR(A \to \tau\tau)$ [pb]
m_A [GeV]

FIG. 9: Cross sections at $\sqrt{s} = 8$ TeV for light A production from gg fusion (top row) and $b\bar{b}$ associated production (bottom row) in the $\tau\tau$ final state. The cross sections for the $\mu\mu$ final state have exactly the same form but are two orders of magnitude lower. Same colour scheme as in the previous figures.

in the Run 1 data set.

Analyses by ATLAS and CMS for such signals at low m_A in the $\tau\tau$ channel have significant background from the Z peak. As a result, limits are currently only available for $m_A \gtrsim m_Z$. We are unaware of any public results for the $\mu\mu$ final state in the low mass region, but the excellent mass resolution in this channel should make separation from the Z peak straightforward.

Finally, we note that running at higher energies will not straightforwardly improve the sensitivity to the low m_A region, as the cross sections at 13–14 TeV are barely a factor 2 larger than those at 8 TeV. Therefore, one will need to accumulate more statistics via higher total integrated luminosity.

III. THE $m_H \sim 125$ GeV CASE

We first note that for $m_H \sim 125$ GeV in the Type II model, B-physics constraints require $m_A \gtrsim 200$ GeV. We therefore only consider the case of $m_h < m_H/2$ for Type II. In contrast, in the Type I model either m_A or m_h can be $< m_H/2$, but LEP limits imply that not both can be light simultaneously. This latter follows from the fact that the HVV coupling and the ZhA coupling are both proportional to $\cos(\beta-\alpha)$. Thus, for a SM-like H, *i.e.* $|\cos(\beta-\alpha)| \sim 1$ as required by signal strengths measurements, the ZhA coupling is near maximal and therefore the $Z^* \to hA$ cross section at LEP is too large, barring phase-space suppression.

In practice we can therefore consider the $H \to AA$ and $H \to hh$ cases independently of one another. With this in mind, we turn to the conditions for achieving small trilinear couplings in order to evade too large $\mathrm{BR}(H \to AA)$ or $\mathrm{BR}(H \to hh)$. Analogous to Eq. (7) we find

$$g_{HAA} = \frac{1}{2v}\left[\left(2m_A^2 - m_H^2\right)\frac{\sin(\alpha-3\beta)}{\sin 2\beta} + \left(8m_{12}^2 - \sin 2\beta\left(2m_A^2+3m_H^2\right)\right)\frac{\sin(\beta+\alpha)}{\sin^2 2\beta}\right] \quad (12)$$

and

$$g_{Hhh} = -\frac{1}{v}\cos(\beta-\alpha)\left[\frac{2m_{12}^2}{\sin 2\beta} + \left(2m_h^2 + m_H^2 - \frac{6m_{12}^2}{\sin 2\beta}\right)\frac{\sin 2\alpha}{\sin 2\beta}\right]. \quad (13)$$

As mentioned, for the H to be SM-like, we should have $|\cos(\beta-\alpha)|$ close to unity. One class of scenarios is easily understood by taking the strict limit of $|\cos(\beta-\alpha)| = 1$, yielding

$$g_{HXX} = -\frac{2m_X^2 + m_H^2 - 2\hat{m}_{12}^2}{v}, \qquad X = h, A. \quad (14)$$

Analogous to the $h125$ case, $\hat{m}_{12}^2 = m_{12}^2 \sec\beta \csc\beta$ should be small and positive to achieve small enough $|g_{HXX}|$. The interplay of the requirements of perturbativity and of small $|g_{HXX}|$ is illustrated in Fig. 10. We see that for $m_h \leq 60$ GeV, small $\tan\beta$ below about 2 is required. (Note also that if both h and A were light, they should be very close in mass to suppress $\mathrm{BR}(H \to hh, AA)$; this follows from the fact that the bands of $\mathrm{BR}(H \to XX) < 0.3$ are valid for both $X = h$ and $X = A$.) For $0.5\,m_H < m_h < m_H$, *i.e.* if only A is light, there is a bit more freedom and $\tan\beta$ can go up to 10–15, tightly related however with m_{12} for any given value of m_A. Figure 10 gives a somewhat idealized picture because the signal strength measurements at 125 GeV only require $C_V \gtrsim 0.9$, and constraints from the oblique

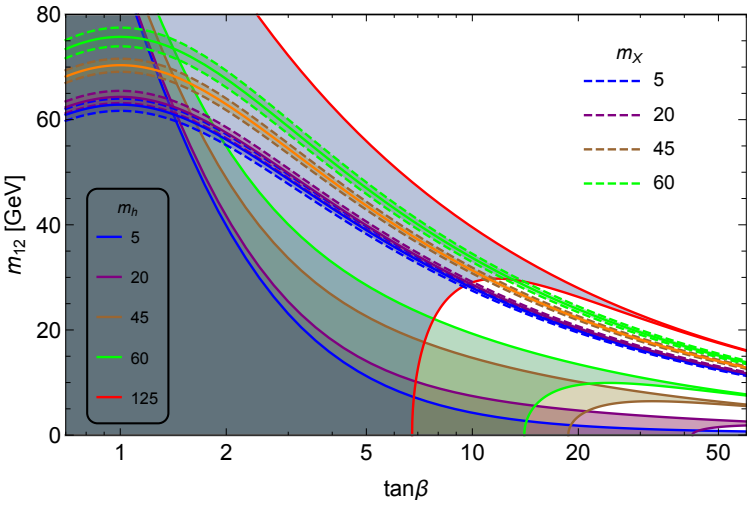

FIG. 10: Constraints in the m_{12} vs. $\tan\beta$ plane for the $H125$ case with $|\cos(\beta-\alpha)| = 1$. The shaded regions are those allowed by perturbativity for m_h values indicated in the lower-left corner of the plot. The narrow strips between the dashed lines have $\mathrm{BR}(H \to XX) < 0.3$ for $m_A < m_H/2$ or $m_h < m_H/2$, respectively (the regions are the same for the two cases) with the colour code for the $X = h$ or A masses given in the upper-right corner of the plot. The solid line in the middle of the dashed ones shows $g_{HXX} = 0$.

parameters STU actually forbid $|\cos(\beta-\alpha)|$ being exactly 1; nonetheless Fig. 10 serves as useful guidance for the parameter scan.

As in the $h125$ case, sufficiently small $|g_{HXX}|$ can also be achieved by resorting to cancellations between the various terms in Eq. (12) or Eq. (13). In the $H125$ case, the $|\cos(\beta-\alpha)| = 1$ component shown in Eq. (14) is positive for larger m_{12} values than those shown in Fig. 10 and this component can be cancelled by the remaining term(s) for $\cos(\beta+\alpha) \sim 1$.

Putting everything together, including also the experimental constraints, we end up with the situation shown in Fig. 11. The top row shows allowed points in the m_{12} vs. $\tan\beta$ plane (analogous to Fig. 10); the bottom row displays these same allowed points in the $\tan\beta$ vs. $\sin\alpha$ plane. As explained at the beginning of this section, in Type I either h or A can be light (but not both) while in Type II only h can be light but not A. To distinguish these two cases, points with $m_A < m_H/2$ are shown in red and points with $m_h < m_H/2$ in blue. Considering first the top row of plots we see that, in agreement with Fig. 10, there is a small allowed region with $m_h < m_H/2$ at $m_{12} \simeq 60$–80 GeV and $\tan\beta \lesssim 2$. This region occurs for

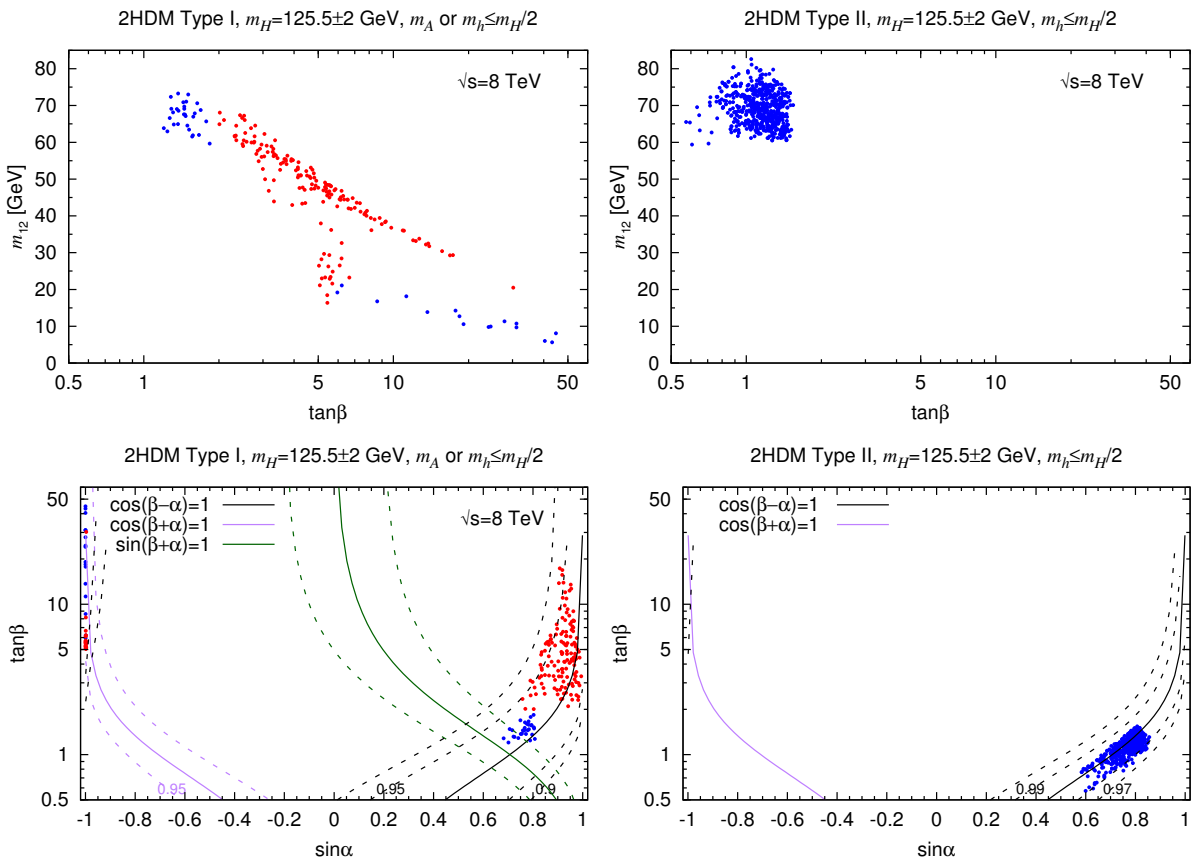

FIG. 11: Phenomenologically viable scan points for the H125 scenario in the Type I (left) and Type II (right) models. The upper row shows the projection onto the m_{12} vs. $\tan\beta$ plane for comparison with Fig. 10. The lower row shows the $\tan\beta$ vs. $\sin\alpha$ plane, including contours of constant $\cos(\beta \pm \alpha)$ and $\sin(\beta + \alpha)$. In all four plots, the red points have $m_A \leq m_H/2$ while the blue points have $m_h \leq m_H/2$. Note that there are no red points for Type II; moreover, there are no $\cos(\beta + \alpha) \sim 1$ points in Type II that pass all constraints.

both Type I and Type II, although it is more constrained in Type I (because of combined SUP+STU constraints). In Type I there is moreover a diagonal strip of allowed points with $m_A < m_H/2$ at $\tan\beta \simeq 2 - 12$, as expected from Fig. 10. The points below this strip are mostly $\cos(\beta + \alpha) \sim 1$ points for which cancellations occur, cf. the lower-left plot of Fig. 11; they can have $m_A < m_H/2$ or $m_h < m_H/2$. Note that no such points survive in Type II. Last, but not least, it is worth noting that, in contrast to the $h125$ case, in the $H125$ case there are no allowed points with "wrong sign" Yukawa couplings, *i.e.* points for which the couplings of the H to vector bosons and to bottom quarks have opposite signs.

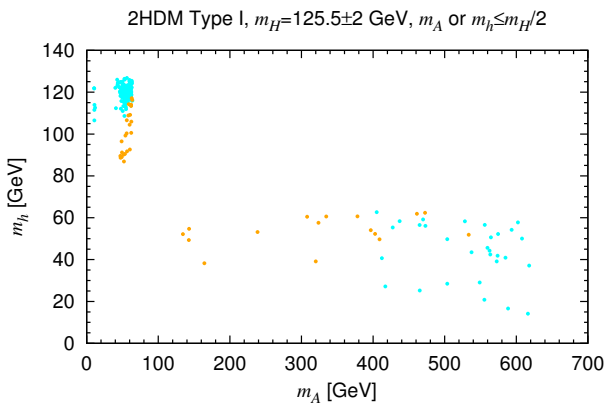

FIG. 12: Allowed $H125$ points for the Type I model in the m_h vs. m_A plane. The cyan points have $\sin\alpha > 0$, while the orange points have $\sin\alpha \sim -1$, cf. the bottom-left plot in Fig. 11.

In Fig. 12, we take a closer look at the allowed points in the m_h vs. m_A plane for Type I. We see that indeed no points survive in the region where both m_h and m_A are below $m_H/2$. As m_h increases, some low m_A points appear, but these correspond to either $m_A \lesssim 12$ GeV for which there are no published limits at large m_h on $e^+e^- \to Z^* \to hA$ or to $m_A \gtrsim 40-50$ GeV and $m_h \gtrsim 90$ GeV *i.e.* sufficiently close to LEP threshold as to escape limits on the hA final state by virtue of suppressed cross section. In the gap from about 15 GeV to about 40 GeV, LEP limits are strong enough to eliminate all points. It is also worth noting that the cyan points with $\sin\alpha > 0$ and the orange points with $\sin\alpha \sim -1$ occupy rather distinct parts of the m_h vs. m_A plane. In particular, if a light scalar with $m_h < 60$ GeV plus a pseudoscalar with $m_A < 400$ GeV were discovered, this would fix $\sin\alpha \sim -1$ in Type I.

Let us now explore the phenomenological consequences of the $H125$ scenario for the LHC. To this end, we first show in Fig. 13 the relation between the signal strengths for the high-resolution channels $gg \to H \to VV$ ($VV = WW^{(*)}, ZZ^{(*)}$) denoted as $\mu^H_{gg}(VV)$ and $gg \to H \to \gamma\gamma$ denoted as $\mu^H_{gg}(\gamma\gamma)$. As in the $h125$ case, quite substantial deviations from the SM values of unity are possible. With the increased precision expected at Run 2, the Higgs measurements at the LHC should be sensitive to such deviations. Moreover, also as in the $h125$ case, the exact SM case $\mu^H_{gg}(\gamma\gamma) = \mu^H_{gg}(VV) = 1$ cannot be obtained in the $H125$ scenarios with light h or A. Though not shown here, this tension with SM-like signal strengths is also apparent in the $\mu^H_{\rm VBF}(\gamma\gamma)$ vs. $\mu^H_{gg}(\gamma\gamma)$ plane. Should the signal strength

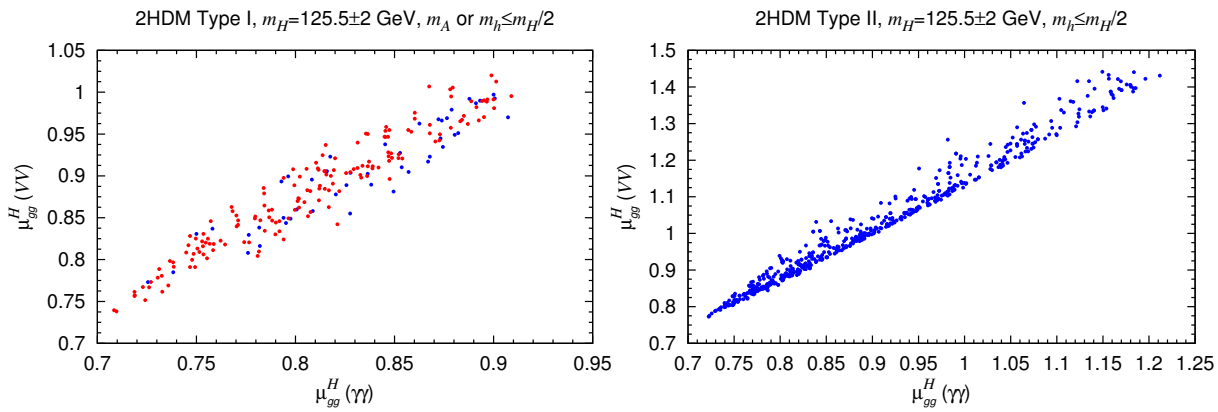

FIG. 13: Signal strengths $\mu^H_{gg}(VV)$ vs. $\mu^H_{gg}(\gamma\gamma)$ for the Type I and Type II models. Points with $m_A \le m_H/2$ are shown in red and points with $m_h \le m_H/2$ in blue.

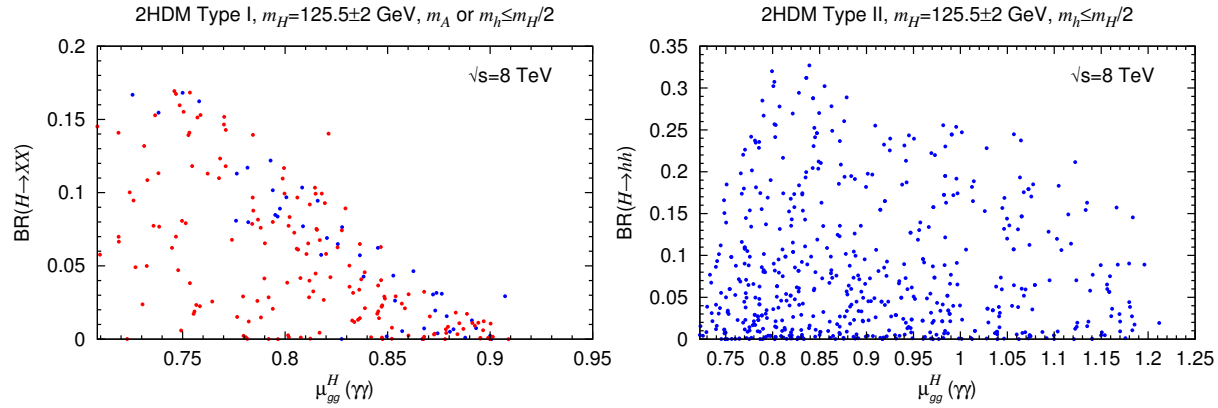

FIG. 14: Branching ratios of $H \to XX$ $(X = h, A)$ decays vs. $\mu^H_{gg}(\gamma\gamma)$ for the Type I and Type II models. Points with $m_A \le m_H/2$ are shown in red and points with $m_h \le m_H/2$ in blue.

measurements for either of these pairs converge to values that lie within 10% of their SM values the $H125$ scenarios with m_h or m_A below $m_H/2$ will be excluded.[6] For completeness we show in Fig. 14 also BR($H \to XX$), $X = h$ or A, versus $\mu^H_{gg}(\gamma\gamma)$. Despite the existing Run 1 constraints, the branching ratios can be sizeable and it may thus be interesting to look for these decays.

The most important issue is whether or not the existing 8 TeV, $L = 20$ fb^{-1} data set could be sensitive to this scenario by looking for the light h or A in the $\tau\tau$ or $\mu\mu$ final states. The relevant plots are given in Fig. 15. Since $\tan\beta$ cannot be large in the Type II model

[6] Comparing with Fig. 7 of [14] we see that this tension with SM-like signal strengths is much less in the general $H125$ case with heavier h, A.

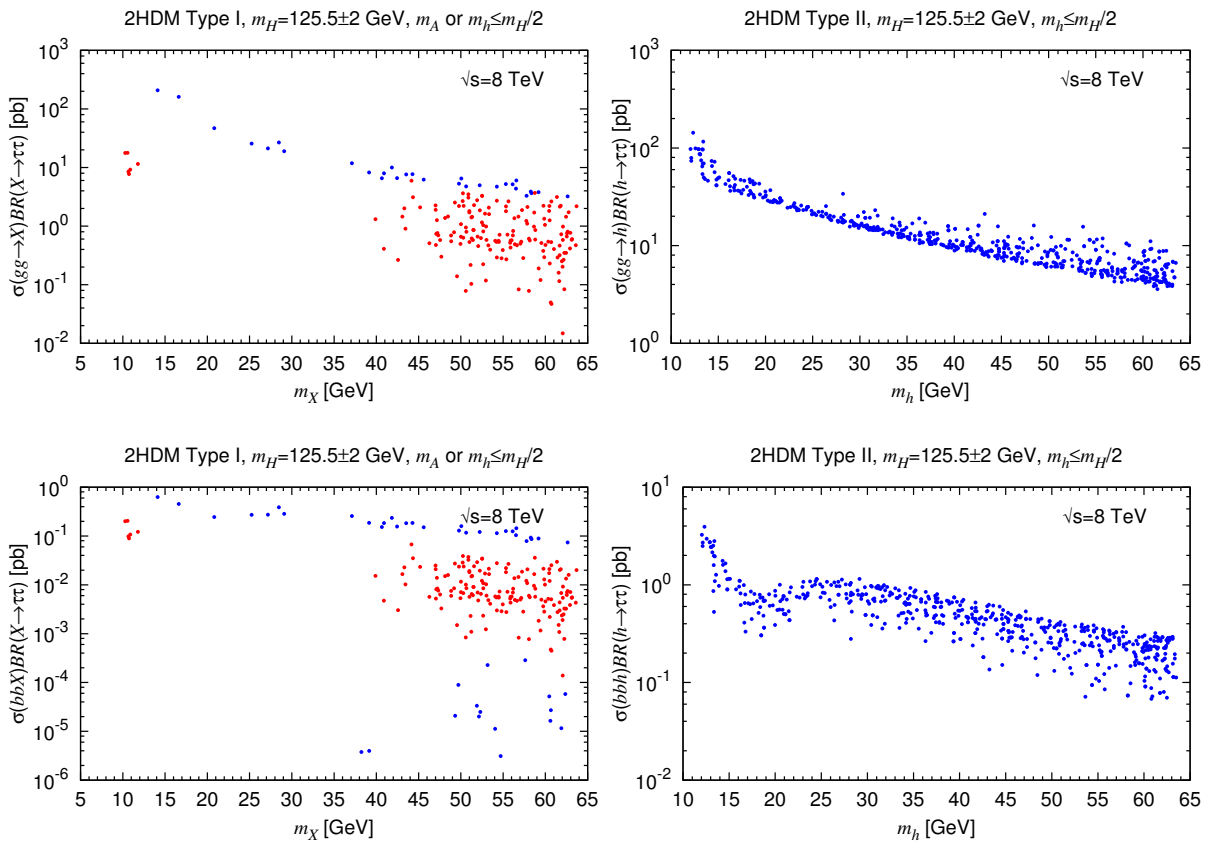

FIG. 15: For the $H125$ case, we give 8 TeV cross sections for light $X = h, A$ production from gg fusion (upper row) and $b\bar{b}$ associated production (lower row) in the $\tau\tau$ final state. The blue points are for $X = h$, the red points for $X = A$.

(see Fig. 11) and there is no $\tan\beta$ enhancement of the $b\bar{b}$ coupling in the Type I model, it is mostly gg fusion that's relevant. $\sigma(gg \to X) \times \mathrm{BR}(X \to \tau\tau)$ exceeds the required 10 pb (or 0.1 pb for decays into $\mu\mu$) in particular for the light h case, $X = h$. Light pseudoscalars (possible only in Type I) have smaller cross sections and will be harder to detect. Concretely, only for gg fusion with $A \to \tau\tau$ and $m_A \lesssim 12$ GeV does one obtain a cross section as large as 10 pb in the $\tau\tau$ channel, though for $m_A > 40$ GeV cross sections are still between 1 pb and 10 pb.

A final comment concerns the issue of vacuum stability in these scenarios. According to [18], the 2HDM minimum is the global minimum only if $D \equiv m_{12}^2(m_{11}^2 - k^2 m_{22}^2)(\tan\beta - k) > 0$, where $k = (\lambda_1/\lambda_2)^{1/4}$. However, given that $D < 0$ may still correspond to a metastable vacuum, we have chosen not to require $D > 0$; one would need to compute the corresponding vacuum lifetime, which is beyond the scope of the present study. We note that were we to

require $D > 0$ this would eliminate only a small percentage of the $h125$ scenario points, but would exclude about 20% of the points in the $H125$ scenario. We leave further investigation of the implications of vacuum (meta)stability to future work.

IV. CONCLUSIONS

We have considered 2HDM scenarios of Type I and Type II in which the A or h has mass below one-half that of the observed 125 GeV SM-like Higgs state, when the latter is identified with either the lighter CP-even h or heavier CP-even H. It turns out that this is a region which LEP limits do not constrain at all in the $h125$ case or only partially constrain in the $H125$ case. The conditions and associated parameter choices for obtaining viable scenarios that have a small enough decay branching ratios of the ~ 125 GeV Higgs boson into a pair of lighter Higgs states were discussed in detail.

Regarding LHC phenomenology, we found that in the scenarios under consideration the signal strengths of the ~ 125 GeV Higgs boson cannot all be SM-like. Should the signal strength measurements in the high-resolution $\gamma\gamma$ and VV channels converge to their SM values to within 10% or better, then these scenarios will be excluded. Moreover, in the $h125$ case, surprisingly large gg fusion and $b\bar{b}$ associated production cross sections are possible for a light pseudoscalar in the 10–60 GeV mass range; naive estimates suggest that these should be readily testable in the $\tau\tau$ and $\mu\mu$ channels using the existing 8 TeV data from Run 1 of the LHC.

Overall, one finds ample motivation from these 2HDM scenarios for the ATLAS and CMS collaborations to explore their sensitivity to Higgs particles with masses below about 60 GeV in the $\tau\tau$ and $\mu\mu$ final states. If sufficient sensitivity is reached and nothing is observed, then many of the 2HDM scenarios explored in this paper will be eliminated. On the other hand, if such a light Higgs is detected then models such as the MSSM will be eliminated and a strong preference in favour of, *e.g.*, a general 2HDM or the NMSSM will arise.

V. ACKNOWLEDGEMENTS

This work was supported in part by US DOE grant DE-SC-000999 and by the French ANR project DMAstroLHC. J.B. is supported by the "Investissements d'avenir, Labex

ENIGMASS". Y.J. is supported by LHC-TI fellowship US NSF grant PHY-0969510; he also thanks the LPSC Grenoble for hospitality and the Labex ENIGMASS for financial support for a research stay during which this work was finished.

---

[1] J. F. Gunion and H. E. Haber, *The CP conserving two Higgs doublet model: The Approach to the decoupling limit*, *Phys.Rev.* **D67** (2003) 075019, [hep-ph/0207010].

[2] J. Gunion and H. E. Haber, *Higgs Bosons in Supersymmetric Models. 1.*, *Nucl.Phys.* **B272** (1986) 1.

[3] L.-F. Li, Y. Liu, and L. Wolfenstein, *Hidden Higgs Particles*, *Phys.Lett.* **B159** (1985) 45.

[4] J. F. Gunion, H. E. Haber, G. L. Kane, and S. Dawson, *THE HIGGS HUNTER'S GUIDE*, *Front.Phys.* **80** (2000) 1–448.

[5] J. Bernon, B. Dumont, and S. Kraml, *Status of Higgs couplings after run 1 of the LHC*, *Phys.Rev.* **D90** (2014), no. 7 071301, [arXiv:1409.1588].

[6] D. Curtin, R. Essig, S. Gori, P. Jaiswal, A. Katz, et al., *Exotic decays of the 125 GeV Higgs boson*, *Phys.Rev.* **D90** (2014), no. 7 075004, [arXiv:1312.4992].

[7] M. Carena, S. Heinemeyer, O. Stl, C. Wagner, and G. Weiglein, *MSSM Higgs Boson Searches at the LHC: Benchmark Scenarios after the Discovery of a Higgs-like Particle*, *Eur.Phys.J.* **C73** (2013) 2552, [arXiv:1302.7033].

[8] D. G. Cerdeno, P. Ghosh, and C. B. Park, *Probing the two light Higgs scenario in the NMSSM with a low-mass pseudoscalar*, *JHEP* **1306** (2013) 031, [arXiv:1301.1325].

[9] J. Cao, F. Ding, C. Han, J. M. Yang, and J. Zhu, *A light Higgs scalar in the NMSSM confronted with the latest LHC Higgs data*, *JHEP* **1311** (2013) 018, [arXiv:1309.4939].

[10] N.-E. Bomark, S. Moretti, S. Munir, and L. Roszkowski, *A light NMSSM pseudoscalar Higgs boson at the LHC redux*, arXiv:1409.8393.

[11] J. Huang, T. Liu, L.-T. Wang, and F. Yu, *Supersymmetric Exotic Decays of the 125 GeV Higgs Boson*, *Phys.Rev.Lett.* **112** (2014), no. 22 221803, [arXiv:1309.6633].

[12] J. F. Gunion, H. E. Haber, and T. Moroi, *Will at least one of the Higgs bosons of the next-to-minimal supersymmetric extension of the standard model be observable at LEP-2 or the LHC?*, *eConf* **C960625** (1996) LTH095, [hep-ph/9610337].

[13] B. Dumont, J. F. Gunion, Y. Jiang, and S. Kraml, *Constraints on and future prospects for Two-Higgs-Doublet Models in light of the LHC Higgs signal*, *Phys.Rev.* **D90** (2014) 035021, [arXiv:1405.3584].

[14] B. Dumont, J. F. Gunion, Y. Jiang, and S. Kraml, *Addendum to "Constraints on and future prospects for Two-Higgs-Doublet Models in light of the LHC Higgs signal"*, arXiv:1409.4088.

[15] "http://lpsc.in2p3.fr/projects-th/lilith".

[16] P. Ferreira, J. F. Gunion, H. E. Haber, and R. Santos, *Probing wrong-sign Yukawa couplings at the LHC and a future linear collider*, *Phys.Rev.* **D89** (2014) 115003, [arXiv:1403.4736].

[17] P. Ferreira, R. Guedes, M. O. Sampaio, and R. Santos, *Wrong sign and symmetric limits and non-decoupling in 2HDMs*, *JHEP* **1412** (2014) 067, [arXiv:1409.6723].

[18] A. Barroso, P. Ferreira, I. Ivanov, and R. Santos, *Metastability bounds on the two Higgs doublet model*, *JHEP* **1306** (2013) 045, [arXiv:1303.5098].